Journal of Inflammation Research

Dovepress
open access to scientific and medical research

Open Access Full Text Article

ORIGINAL RESEARCH

Pan-Cancer Screening and Validation of CALU's Role in EMT Regulation and Tumor Microenvironment in Triple-Negative Breast Cancer

Shi-liang Chen[1,*], Dan Hu[2,*], Tian-zhu Chen[3,*], Si-yu Shen[4,*], Chen-fei Zhao[1,*], Cong Wang[1], Shi-yuan Tong[5], Zhao Liu[6], Shao-hua Lin[1], Li-xia Jin[7], Yi-bo He[1], Zhe-zhong Zhang[1]

[1]Department of Clinical Lab, The First Affiliated Hospital of Zhejiang Chinese Medical University (Zhejiang Provincial Hospital of Chinese Medicine), Hangzhou, People's Republic of China; [2]Department of Clinical Lab, The Cixi Integrated Traditional Chinese and Western Medicine Medical and Health Group Cixi Red Cross Hospital, Cixi, People's Republic of China; [3]Department of Pathology, The First Affiliated Hospital of Zhejiang Chinese Medical University (Zhejiang Provincial Hospital of Chinese Medicine), Hangzhou, People's Republic of China; [4]The First School of Clinical Medicine, Zhejiang Chinese Medical University, Hangzhou, People's Republic of China; [5]The Key Laboratory of Medical Neurobiology and MOE Frontiers Center for Brain Science, Institutes of Brain Science, Fudan University, Shanghai, People's Republic of China; [6]Department of General Surgery, Shaoxing Central Hospital, Shaoxing, People's Republic of China; [7]School of Medical Technology and Information Engineering, Zhejiang Chinese Medical University, Hangzhou, People's Republic of China

*These authors contributed equally to this work

Correspondence: Zhe-zhong Zhang; Yi-bo He, Department of Clinical Lab, The First Affiliated Hospital of Zhejiang Chinese Medical University (Zhejiang Provincial Hospital of Chinese Medicine), Hangzhou, People's Republic of China, Email zhangzhezhong2023@163.com; heyb1992@126.com

Purpose: Cancer-associated fibroblasts (CAFs) significantly contribute to tumor progression and the development of resistance to therapies across a range of malignancies, notably breast cancer. This study aims to elucidate the specific role and prognostic relevance of CALU across multiple cancer types.

Patients and Methods: The association between CALU expression and prognosis, along with clinical characteristics in BRCA, HNSC, KIRP, LGG, and LIHC, was analyzed using data from the TCGA, GTEx, and GEO databases. Transcriptomic analysis of TCGA BRCA project data provided insights into the interaction between CALU and epithelial-mesenchymal transition (EMT) marker genes. Using TIMER and TISCH databases, the correlation between CALU expression and tumor microenvironment infiltration was assessed, alongside an evaluation of CALU expression across various cell types. Furthermore, CALU's influence on TNBC BRCA cell lines was explored, and its expression in tumor tissues was confirmed through immunohistochemical analysis of clinical samples.

Results: This study revealed a consistent upregulation of CALU across several tumor types, including BRCA, KIRP, LIHC, HNSC, and LGG, with elevated CALU expression being associated with unfavorable prognoses. CALU expression was particularly enhanced in clinical contexts linked to poor outcomes. Genomic analysis identified copy number alterations as the principal factor driving CALU overexpression. Additionally, a positive correlation between CALU expression and CAF infiltration was observed, along with its involvement in the EMT process in both CAFs and malignant cells. In vitro experiments demonstrated that CALU is highly expressed in TNBC-BRCA cell lines, and knockdown of CALU effectively reversed EMT progression and inhibited cellular migration. Immunohistochemical analysis of clinical samples corroborated the elevated expression of CALU in tumors, along with alterations in EMT markers.

Conclusion: This comprehensive pan-cancer analysis underscores CALU's critical role in modulating the tumor microenvironment and facilitating cell migration via the EMT pathway, identifying it as a potential therapeutic target.

Keywords: CALU, cancer-associated fibroblasts, epithelial-mesenchymal transition, breast cancer, prognosis, pan-cancer analysis

Received: 11 July 2024
Accepted: 20 September 2024
Published: 25 September 2024

Introduction

Cancer remains a critical global health challenge, contributing to a substantial number of fatalities and imposing significant economic burdens.[1] Despite the availability of various treatment modalities, including surgery, chemoradiotherapy, targeted therapy, and immunotherapy, the prognosis for many patients with cancers remains poor due to challenges such as drug resistance and adverse treatment effects.[2,3] As a result, there is an urgent need to identify novel therapeutic targets and diagnostic biomarkers to improve cancer treatment outcomes. The tumor microenvironment (TME) is known to play a pivotal regulatory role in breast cancer progression and metastasis.[4] Within the TME, Cancer-associated fibroblasts (CAFs) have garnered considerable attention for their role in breast cancer.[4–7] Targeting CAFs may provide a promising strategy for controlling breast cancer progression and overcoming therapeutic resistance.[8] CAFs, as a major stromal component of the TME, engage in dynamic interactions with tumor-infiltrating immune cells and other immune constituents through the secretion of a broad spectrum of cytokines, growth factors, and chemokines.[9]

Calumenin (CALU), a calcium-binding protein belonging to the CREC family, plays diverse roles in cellular processes, including chaperone function,[10] calcium homeostasis,[11] secretory cargo sorting,[12] cell proliferation,[13] and cell migration.[14] Multiple studies have demonstrated an association between elevated CALU expression and cancer metastasis. Nagano et al reported significantly higher CALU expression in metastasis-positive lung tissues compared to metastasis-negative counterparts.[15] Likewise, Kunita et al found that CAF-secreted CALU was linked to enhanced lung cancer cell proliferation.[16] Beyond lung cancer, CALU has also been implicated in promoting metastasis in colon cancer, as Nasri Nasrabadi et al showed its role as a metastasis promoter in both colon and lung cancers.[17]

CALU also plays a critical role in the crosstalk between tumor cells and the TME. Vorum et al[18] identified CALU expression in the endoplasmic reticulum and Golgi apparatus of MRC-5 fibroblasts, while Hansen et al[19] demonstrated that CALU encodes secreted isoforms of the CALU protein. Furthermore, Østergaard et al[20] suggested that CALU may exert autocrine or paracrine effects, influencing processes such as cytoskeletal rearrangement and cell proliferation. These results imply that secreted CALU isoforms may modulate the TME by altering cell proliferation and migration dynamics. Kunita et al[16] observed that A549 cells secrete TGFβ, which induces the transformation of fibroblasts like IMR-90 and MRC-50 into CAFs. Simultaneously, TGFβ drives the upregulation of CALU in fibroblasts via MicroRNA-21, thereby enhancing the proliferation and migration of A549 cells. These insights underscore CALU's central role in the reciprocal regulation between tumor cells and CAFs. However, the function of CALU in breast cancer and other malignancies remains insufficiently characterized.

Recent research has demonstrated a strong association between CALU and Epithelial-Mesenchymal Transition (EMT).[21,22] EMT serves as a fundamental process driving tumor invasion and metastasis.[23,24] Stromal cells are a critical source of EMT-associated gene expression, further influencing responses to immune checkpoint blockade (ICB) therapy and impacting patient survival by modulating T cell infiltration across multiple cancer types.[25] Available evidence suggests that EMT is a complex, interdependent interaction between cancer cells and stromal components,[26] leading to the acquisition of a mesenchymal phenotype in cancer cells and consequently enhancing their invasive and metastatic capabilities.[25] However, most studies on CALU's role in tumors are confined to specific cancer types, and a comprehensive pan-cancer investigation of CALU's correlation with different cancers is lacking. To address this, various data repositories were utilized to analyze CALU expression levels and its prognostic significance across different malignancies, including TCGA, Genotype Tissue-Expression (GTEx), Cancer Cell Line Encyclopedia (CCLE), cBioPortal, and the Human Protein Atlas (HPA).

Given the strong association between CALU, CAFs, and EMT, a comprehensive analysis was performed to explore CALU's relationship with EMT across different tumors using transcriptome data from TCGA. Single-cell sequencing data from the TISCH database were also employed to validate the interactions between CALU and various cell types within the TME. The results suggest that CALU has significant potential as a prognostic biomarker in multiple cancers and plays a critical role in facilitating stromal cell-mediated tumor migration, particularly involving CAFs. A summary of the analysis workflow is provided in Figure 1.

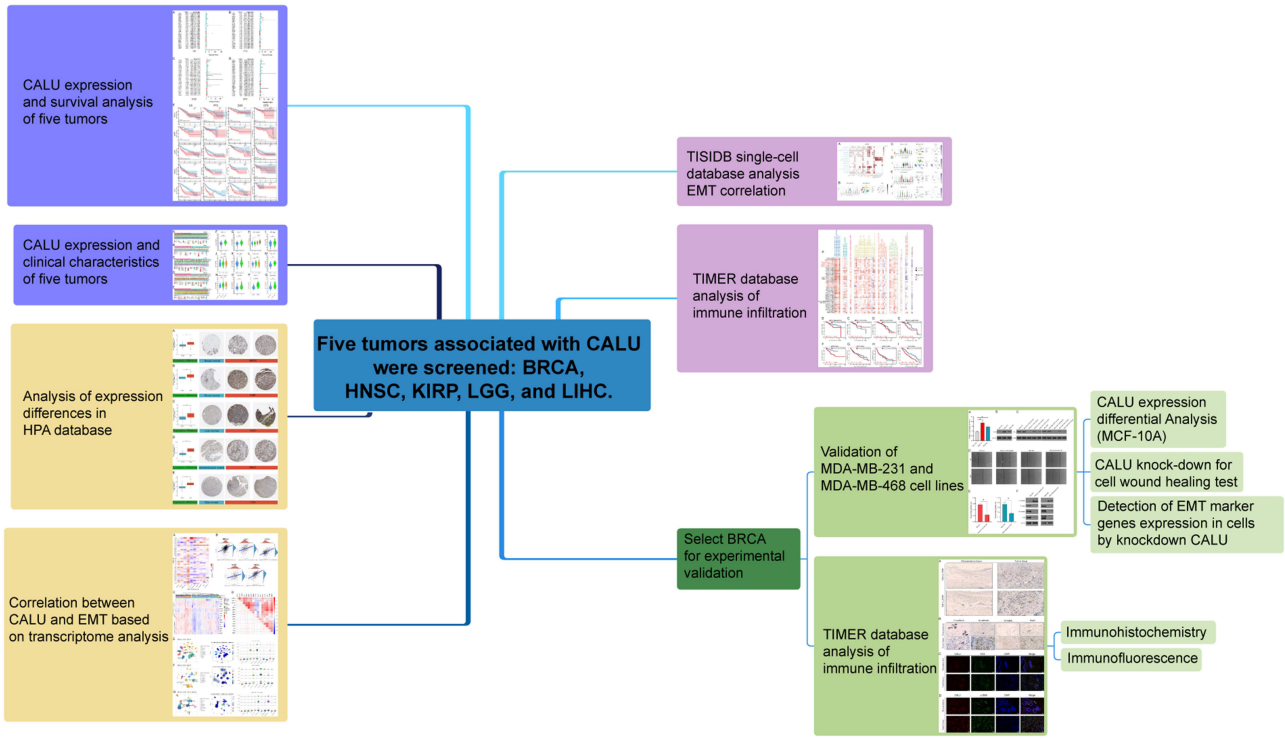

Figure 1 The flowchart of our study.

Materials and Methods

Data Processing and Expression Analysis

RNA-seq, somatic mutation, and clinical data were obtained from TCGA through the University of California Santa Cruz (UCSC) Xena browser (https://xenabrowser.net/). Similarly, GTEx transcription expression RNA-seq and phenotype data were accessed via the Xena browser, with CALU expression analyzed across 31 different tissues. Furthermore, RNA-seq data from the Gene Expression database of Normal and Tumor tissues (GENT2, http://gent2.appex.kr/gent2) were utilized to assess CALU expression in various solid tumors and hematologic malignancies. Data from the Cancer Cell Line Encyclopedia (CCLE, https://portals.broadinstitute.org/ccle/) were also leveraged for tumor cell line analysis. Sequencing data were log2 transformed, and Wilcoxon tests were applied to compare CALU expression between normal and tumor samples from multiple cancers. Additional analyses utilized the TIMER database (https://cistrome.shinyapps.io/timer/) to examine CALU expression and immune infiltrate abundance across pan-cancer datasets. Single-cell sequencing data were sourced from the TISCH database (http://tisch.comp-genomics.org/home/).

Survival and Clinical Phenotypes Analysis of CALU

Survival analysis was performed to evaluate the correlation between CALU expression and patient prognosis, covering overall survival (OS), disease-specific survival (DSS), disease-free survival (DFS), and progression-free survival (PFS). Kaplan-Meier survival curves were generated using the Kaplan-Meier method and Log rank test, with visualization achieved through the R packages "survival" and "survminer". Additionally, the Cox proportional hazard regression model was applied to examine the association between CALU expression and survival outcomes, with results visualized using "survival" and "forestplot" R packages. A heatmap of clinical attributes was created using the "pheatmap" package.

Inclusion and Exclusion Criteria

To identify tumors with the highest research value for CALU, two screening criteria were applied. First, CALU had to demonstrate significant differential expression ($p < 0.05$) between tumor and normal samples in at least three of the four

databases: TCGA+GTEx, TIMER2.0 (TCGA), GENT2 (GPL96), and GENT2 (GPL970). Second, survival analysis had to reveal significant differences ($p < 0.05$) in OS, PFS, DSS, and DFS between high and low CALU expression groups. For the tumors that met these criteria, subsequent survival analyses were conducted using the optimal cutoff method. These stringent criteria ensured that the selected tumors displayed stable CALU expression differences across multiple datasets, while also demonstrating statistical significance in survival analysis, thus enhancing the reliability and accuracy of the findings.

Protein Analysis of CALU

To assess differences in CALU protein expression, immunohistochemistry (IHC) images of normal and tumor tissues—including low-grade glioma (LGG), liver hepatocellular carcinoma (LIHC), breast invasive carcinoma (BRCA), kidney renal papillary cell carcinoma (KIRP), and head and neck squamous cell carcinoma (HNSC)—were analyzed using data from HPA (http://www.proteinatlas.org/).

Mutation, DNA Copy Number, and Methylation Analysis of CALU

Additionally, DNA copy number, methylation, and mutation data were retrieved from the cBioPortal database (http://www.cbioportal.org), with the mutation mapper tool used to visualize the distribution of mutations. The UCSC online tool (https://xenabrowser.net/heatmap/) and GraphPad Prism 8.0 were employed to explore the relationship between CALU gene copy number and methylation.

Biological Significance Analysis of CALU

Gene set enrichment analysis (GSEA) and gene set variation analysis (GSVA) were performed to investigate the biological roles of CALU in tumorigenesis. To explore CALU-associated pathways, samples from each tumor type were stratified into two groups based on the Fraction of Positive Index (FPI), representing the top 30% and bottom 30% of samples. GSEA was then conducted, and functional analysis was performed using R packages such as "limma", "clusterProfiler", and "enrichplot". GSVA scores were calculated for all tumors, and the samples were dichotomized into high and low expression groups using the median expression levels of differentially expressed genes with the R package "limma".

Validation of CALU Expression in BRCA Cell Lines by qRT-PCR

The MCF10A human breast epithelial cell line and the TNBC BRCA cell lines MDA-MB-231 and MDA-MB-468 were obtained from the Cell Bank of the Chinese Academy of Medical Sciences. Total RNA extraction from these cell lines was carried out using the RNeasy Mini Kit (ASPEN, USA). To ensure precision, all samples were analyzed in triplicate, with GAPDH serving as an internal control for normalization. The relative expression levels were determined using the $2^{-\Delta\Delta CT}$ method with the following primers: human CALU, 5"-TGGATTTACGAGGATGTAGAGC-3" (F) and 5"-TTTTAAACCTCCGCTCATCTCT-3" (R); GAPDH, 5"-AGCCACATCGCTCAGACAC-3" (F) and 5"-GCCCAATACGACCAAATCC-3" (R).

In vitro Functional Assays: Transfection

MDA-MB-231 and MDA-MB-468 cells were transfected with either small interfering RNA targeting CALU (siRNA-CALU) or non-silencing control siRNA, following the manufacturer's protocol. siRNAs and negative controls were synthesized by ELK Biotechnology (Wuhan, China), with siRNA sequences targeting CALU as follows: siR-CALU#1, 5"-GAAGGACCGTGTACATCAT-3"; siR-CALU#2, 5"-GTGACAAGGTTCACAATGA-3"; siR-CALU#3, 5"-GACCTTTGATCAGCTGACA-3". The negative control sequence (siR-CALU-NC) was 5"-GCCAAGATCGAGTACGTAT-3". Cell suspensions at a concentration of 1×10^5 cells/mL were seeded into 96-well plates containing 100 μL of complete culture medium per well. After reaching approximately 80% confluence, siRNA was transfected using Lipofectamine 2000, followed by incubation at 37°C for 48 hours.

In vitro Functional Assays: Wound Healing Assay

Post-transfection, approximately 3.5×10^5 cells were plated in 6-well plates and cultured until full confluence. A vertical wound was created in each well using a pipette tip, and cells were cultured in serum-free medium, with three replicates per group. Wound images were captured at 0 and 24 hours after wound formation using a light microscope (CX-21, OLYMPUS, Japan), and migration data were analyzed using Image J 1.8.0 software.

Quantitive PCR and Western Blot Analysis

Real-time fluorescence quantitative PCR (RT-PCR) was performed using the Life Technologies QuantStudio6 Flex System PCR instrument, with three replicate wells per sample, employing the EnTurbo SYBR Green PCR SuperMix kit (ELK Biotechnology, EQ001). The primers used in this assay were as follows: human CALU, 5"-TGGATTTACGAGGATGTAGAGC-3" (F), 5"-TTTTAAACCTCCGCTCATCTCT-3" (R); GAPDH, 5"-AGCCACATCGCTCAGACAC-3" (F), 5"-GCCCAATACGACCAAATCC-3" (R).

Total protein from various cell lines was extracted using RIPA lysis buffer (AS1004, ASPEN), and protein concentration was quantified with the BCA assay kit (AS1086, ASPEN). Subsequently, 40 μg of total protein per sample was separated by SDS-PAGE (AS1012, ASPEN) and transferred onto PVDF membranes (IPVH00010, Millipore). The membranes were blocked in 5% skim milk for two hours and then incubated with primary antibodies, including CALU (1:1000, ab137019, 48 kD, Abcam, CA, USA), Snail (1:1000, #3879, 29 kD, CST), Vimentin (1:3000, #5741, 57 kD, CST), N-Cadherin (1:1000, #4061, 140 kD, CST), E-Cadherin (1:1000, #14472, 135 kD, CST), and β-actin (1:10,000, 43 kD, TDY051, TDY BIOTECH). The following day, membranes were incubated with secondary antibodies, including goat anti-mouse (1:10,000, AS1106, ASPEN), goat anti-rabbit (1:10,000, AS1107, ASPEN), and donkey anti-goat (1:10,000, AS1108, ASPEN), for one hour. Membranes were then incubated with assay buffer (AS1027, ASPEN) for one minute. Protein markers for the Western blot were from TransGen Biotech (catalog number DM211). The membranes were tightly adhered to Kodak Medical X-ray Film (XBT-1, Kodak) and processed in a darkroom using enhanced chemiluminescence (ECL, AS1059, ASPEN) to detect protein signals. Detection was performed using the Image Lab System 3.0 (Bio-Rad, Hercules), and each sample underwent three independent experimental replicates.

Immunohistochemistry and Immunofluorescence

Formalin-fixed, paraffin-embedded (FFPE) tissues from patients with breast cancer were obtained from the pathology department for IHC and immunofluorescence (IF) staining. All procedures were approved by the Ethics Committee of the First Affiliated Hospital of Zhejiang Chinese Medical University, in compliance with the principles of the Helsinki Declaration. Tissue sections were dewaxed, rehydrated, and subjected to heat-induced epitope retrieval. Hydrogen peroxide was applied to block endogenous peroxidase activity, and serum was used to prevent nonspecific binding. The sections were incubated overnight at 4°C with primary antibodies against CALU, E-cadherin, N-cadherin, Snail, and Vimentin (Proteintech, China). After washing, the sections were treated with horseradish peroxidase-conjugated secondary antibodies, stained with diaminobenzidine, and counterstained with hematoxylin. Positive marker staining was observed under a microscope (Nikon, Japan).

Paraffin-embedded sections were first deparaffinized and rinsed in distilled water. Antigen retrieval was conducted by placing the sections in 0.01M citrate buffer (pH 6.0) and heating via microwave. Primary antibodies, including CALU (1:100, Rabbit, PTG, 17804-1-AP), α-SMA (1:400, Mouse, Boster BM0002), and CD3 (1:200, Mouse, PTG, 60181-1-Ig), were diluted with 5% BSA and applied to the sections, which were incubated overnight at 4°C. The sections were then brought to room temperature and washed three times with PBS for 5 minutes each. Subsequently, the appropriate secondary antibody working solution was applied, and the sections were incubated in a water bath at 37°C for 40 minutes in the dark, followed by three PBS washes. DAPI was added for nuclear staining, and after incubation in the dark at room temperature for 20 to 30 minutes, the sections were washed with PBS. Finally, the sections were sealed using an anti-fade mounting medium for fluorescence microscopy observation and imaging. For cell staining, the culture medium was discarded, followed by three PBS washes for 5 minutes each. Cells were fixed with 4% paraformaldehyde for 20 minutes and washed again with PBS. The primary antibody working solution, diluted in 5% BSA, was added to the cells, and incubation was carried out overnight at 4°C. The sections were subsequently warmed, washed with PBS, and incubated

with secondary antibodies in a 37°C water bath in the dark for 40 minutes. DAPI was then applied for nuclear staining, followed by room temperature incubation for 20 to 30 minutes. After washing with PBS, the sections were sealed with an anti-fade mounting medium for fluorescence microscopy observation. The immunohistochemistry staining results were evaluated by experienced pathologists, with scoring categorized as negative (0), weak positive (1), positive (2), and strong positive (3). The final scores from the peritumoral area and tumor core were statistically analyzed for differences between the two groups using a non-parametric test.

Statistical Analysis

Gene expression data were log2-transformed to ensure normalization. A two-tailed *t*-test was employed to compare expression levels between normal and cancer tissues. Kaplan-Meier curves and Cox regression models were used for survival analyses, and correlations between variables were assessed using either Pearson's or Spearman's test. Statistical significance was defined as $*p < 0.05$, $**p < 0.01$, and $***p < 0.001$. All statistical analyses were conducted using R software (version 4.1.3), with graphs generated using GraphPad Prism 8.0, Sangerbox[27] (http://sangerbox.com/), and R software (version 4.1.3).

Results

CALU Exhibits Elevated Transcription Levels in the Majority of Tumors

mRNA sequencing data from the TCGA and GTEx datasets were combined to assess the expression differences between 33 tumor types and normal tissues. *CALU* expression was significantly upregulated in most tumors compared to normal tissues (Figure 2A, $p < 0.05$). Further analysis of mRNA expression differences in the GENT2 and TIMER2.0 databases confirmed these results (Figure 2B–D). Detailed differential expression of *CALU* across various tumors, based on the GENT2 GPL570 and GPL96 platforms, is presented in Supplementary Table 1.

High Expression of CALU is a Poor Prognostic Factor for BRCA, KIRP, LIHC, HNSC, and LGG

Survival association analyses were conducted for OS, DSS, PFS, and DFS to explore the correlation between *CALU* expression and patient prognosis. Cox regression model results indicated that *CALU* expression was significantly associated with OS in LGG, MESO, BLCA, LIHC, CESC, UVM, KIRP, and HNSC (Figure 3A, $p < 0.05$). Additionally, *CALU* expression was notably linked to DSS in PAAD, CESC, PRAD, and LIHC (Figure 3B, $p < 0.05$), as well as to PFS in LGG, CESC, LIHC, MESO, UVM, BRCA, KICH, HNSC, ACC, and LUSC (Figure 3C, $p < 0.05$). Significant associations between *CALU* expression and DFS were observed in LGG, MESO, LIHC, UVM, HNSC, BLCA, KIRP, CESC, and BRCA (Figure 3D, $p < 0.05$). In all tumors, higher *CALU* expression exhibited a greater hazard ratio (HR) according to TCGA data (Figure 3A–D).

Tumors showing differential *CALU* expression in at least three of the following databases—TCGA+GTEx, TIMER2.0, GENT2 (GPL96), and GENT2 (GPL970)—and demonstrating significant differences in at least two survival indicators (OS, PFS, DSS, and DFS) were selected for further analysis. As a result, BRCA, HNSC, KIRP, LGG, and LIHC were chosen for in-depth study (Tables 1 and 2). Kaplan-Meier (KM) survival analysis revealed that high *CALU* expression was associated with poorer OS in LGG, KIRP, LIHC, and HNSC ($p < 0.05$), as well as lower PFS in LIHC, LGG, BRCA, and HNSC ($p < 0.05$). Furthermore, higher *CALU* expression correlated with worse DSS in LGG, LIHC, KIRP, and HNSC ($p < 0.05$). In conclusion, elevated *CALU* expression is a negative prognostic factor in BRCA, KIRP, LIHC, HNSC, and LGG.

CALU Protein Levels are Elevated in Tumor Tissues of BRCA, KIRP, LIHC, HNSC, and LGG

To evaluate the protein expression of *CALU* in these five tumor types, IHC results for BRCA, KIRP, LIHC, HNSC, and LGG, along with corresponding normal tissues, were obtained from the HPA database. These results were cross-referenced with additional mRNA expression data from the same tumors. Data analysis from both databases yielded consistent results

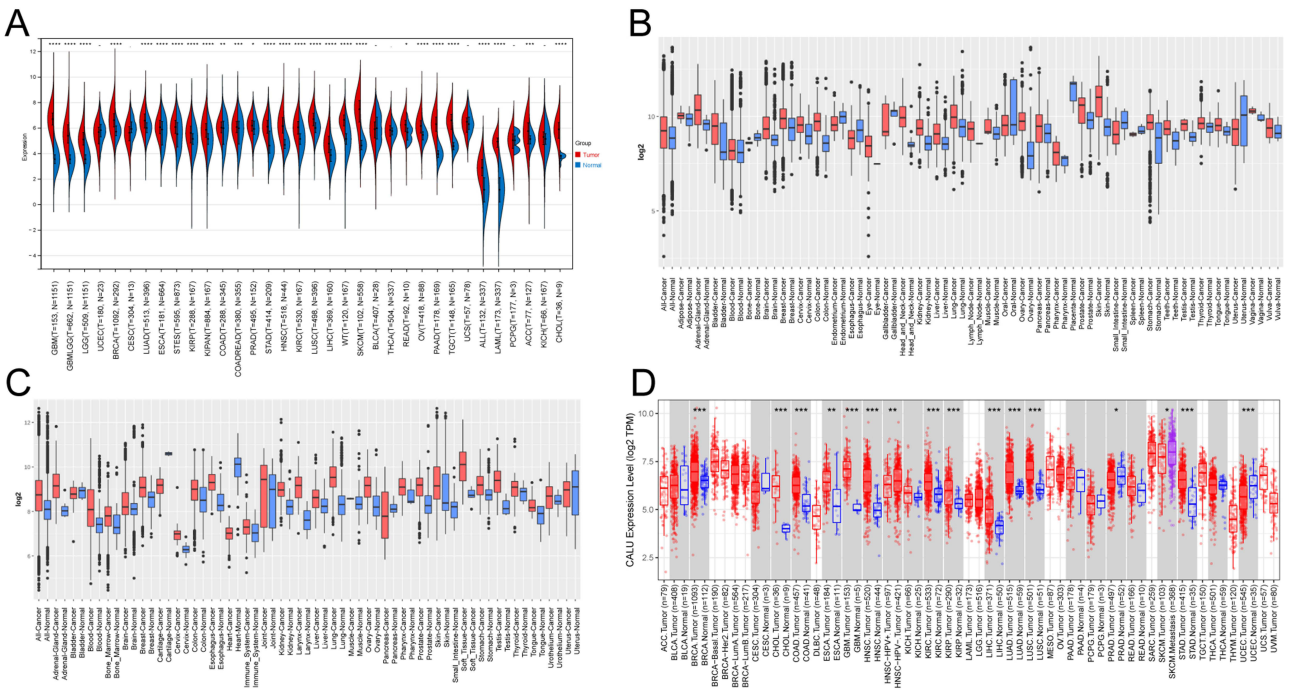

Figure 2 CALU mRNA expression levels in different tumors. (**A**) TCGA+GTEx: CALU expression is elevated in most tumor tissues, except in UCEC, CESC, BLCA, THCA, UCS, PCPG, and KICH. (**B**) GENT2 (GPL570): CALU expression is increased in tumor tissues of the colon, brain, kidney, skin, lung, breast, ovary, liver, stomach, thyroid, head and neck, adrenal gland, bladder, prostate, blood, pancreas, tongue, teeth, and adipose. However, its expression is decreased in endometrium, uterus, esophagus, and bone tumors. (**C**) GENT2 (GPL96): Elevated CALU expression is observed in tumor tissues of the adrenal gland, blood, bone marrow, brain, breast, cervix, colon, esophagus, immune system, kidney, liver, lung, ovary, prostate, soft tissue, stomach, and testis. Decreased expression is noted in cartilage and heart tumors. (**D**) TIMER (TCGA): CALU expression is upregulated in BRCA, CHOL, COAD, ESCA, GBM, HNSC, KIRC, KIRP, LIHC, LUAD, LUSC, and STAD tumors, and downregulated in PRAD and UCEC. Notably, CALU expression is lower in HNSC HPV+ patients compared to HPV- patients, and higher in metastatic SKCM compared to non-metastatic SKCM. Red signifies the presence of neoplastic tissue, blue indicates the presence of healthy tissue, and purple denotes the existence of metastatic tissue. *p< 0.05; **p< 0.01; ***p< 0.001.

(Figure 4A–E, $p < 0.05$). Normal brain, liver, breast, kidney, and skeletal muscle tissues exhibited weak *CALU* IHC staining, while strong staining was observed in LGG, LIHC, BRCA, KIRP, and HNSC tumors (Figure 4A–E).

CALU Exhibits Higher Expression in Tumor Subtypes with Poor Prognosis

A comprehensive analysis was conducted to assess the relationship between *CALU* expression and various clinical features across five tumor types. Figure 5A–E illustrate the clinical features, with statistical significance in *CALU* expression levels denoted by "*". Further examination of *CALU* expression in individual tumors and their clinical characteristics is shown in Figure 5F–Q. In BRCA, higher *CALU* expression was observed in estrogen receptor (ER)-negative and progesterone receptor (PR)-negative cases (Figure 5F–G, $p < 0.0001$). Additionally, *CALU* expression was most pronounced in the Basal subtype, followed by Her2, with LumA and LumB subtypes showing the lowest levels (Figure 5H, $p < 0.0001$). In KIRP, elevated *CALU* expression was significantly associated with advanced tumor stages (Figure 5I, $p < 0.01$). Similarly, in LIHC, higher *CALU* expression was correlated with increased tumor grade and stage (Figure 5J–K, $p < 0.01$). In HNSC, *CALU* expression was higher in HPV-negative patients (Figure 5M, $p < 0.0001$), with the highest expression observed in tongue tumors compared to those in the floor of the mouth and other locations (Figure 5N, $p < 0.01$). In LGG, elevated *CALU* expression was linked to higher tumor grading (Figure 5O, $p < 0.05$), and patients with *IDH* wild-type and unmethylated MGMT exhibited higher *CALU* expression compared to those with IDH mutations and MGMT methylation (Figure 5P–Q, $p < 0.05$).

Genetic Alteration, DNA Methylation, and Gene Copy Number Analysis of CALU

CALU gene alteration patterns and frequencies were examined across various tumor types using cBioPortal. Most tumors exhibited elevated *CALU* mRNA levels, with the exception of mature B-cell tumors. Copy number amplification was the

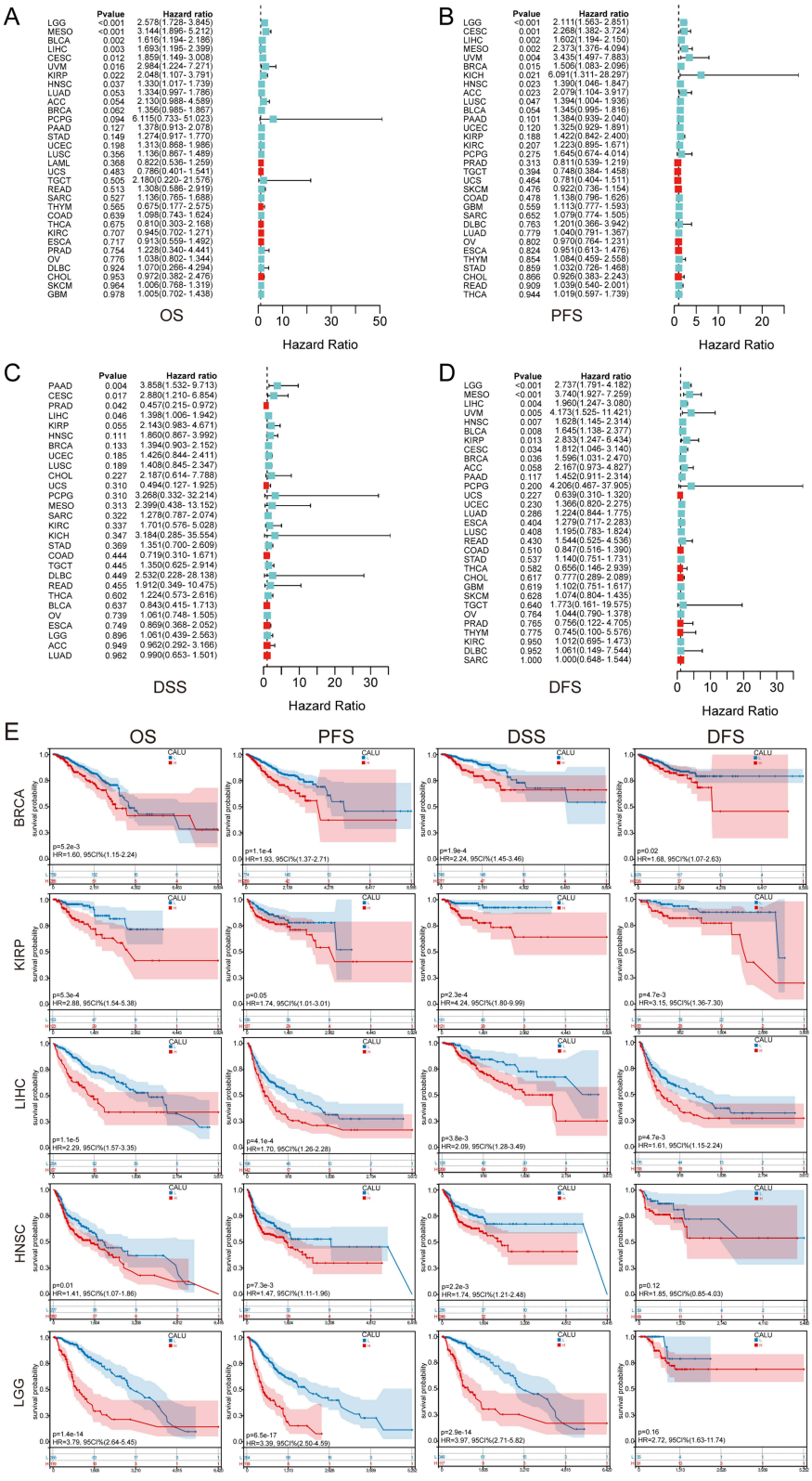

Figure 3 CALU Prognostic analysis of different tumors. (**A**) Overall survival (OS), (**B**) Progression-Free Survival (PFS), (**C**) Disease-Specific Survival (DSS), (**D**) Disease-Free Survival (DFS), and (**E**) Kaplan-Meier analysis of CALU in BRCA, KIRP, LIHC, HNSC, and LGG for different survival indicators.

Table 1 Differential Expression Analysis of Different Tumors in 4 Databases

Cancer	TCGA & GTEx	TIMER (TCGA)	GPL96 (GEO)	GPL570 (GEO)
LIHC	<0.0001	<0.001	<0.001	<0.001
LGG	<0.0001	NA	<0.001	<0.001
MESO	NA	NA	NA	NA
BLCA	NS	NS	0.325	<0.001
CESC	NS	NS	<0.001	0.128
UVM	NA	NA	NA	NA
HNSC	<0.0001	<0.001	NA	<0.001
BRCA	<0.0001	<0.001	<0.001	<0.001
KIRP	<0.0001	<0.001	<0.001	<0.001

Notes: The data in the table represent the p-value of the statistical analysis (two-tailed *t*-test). This table shows the differential analysis of CALU expression between tumor and normal tissue in different tumors, shown as p-values.

Abbreviations: LIHC, Liver Hepatocellular Carcinoma; LGG, Brain Lower Grade Glioma; MESO, Mesothelioma; BLCA, Bladder Urothelial Carcinoma; CESC, Cervical squamous cell carcinoma and endocervical adenocarcinoma; UVM, Uveal Melanoma; HNSC, Head and Neck squamous cell carcinoma; BRCA, Breast invasive carcinoma; KIRP, Kidney renal papillary cell carcinoma; NA, Not Available; NS, No significance.

Table 2 Results of CALU Expression and Survival Analysis in Different Tumors in the TCGA

Cancer	OS	DSS	PFS	DFS
LIHC	0.003	0.004	0.002	0.046
LGG	<0.001	<0.001	<0.001	0.896
MESO	<0.001	<0.001	0.002	0.313
BLCA	0.002	0.008	0.054	0.637
CESC	0.012	0.034	0.001	0.017
UVM	0.016	0.005	0.004	–
HNSC	0.037	0.007	0.0023	0.111
BRCA	0.062	0.036	0.015	0.133
KIRP	0.022	0.013	0.188	0.055
ACC	0.054	0.058	0.023	0.949
KICH	–	–	0.021	0.347
LUSC	0.356	0.408	0.047	0.189
PAAD	0.127	0.117	0.101	0.004
PRAD	0.754	0.765	0.313	0.042

Notes: The data in the table represent the p-value of the statistical analysis (Log rank test). The Cox proportional hazards regression model was constructed using the "coxph" function from the R software package survival (version 3.2–7). Patients were divided into high and low expression groups using the median CALU expression as the cutoff value, and survival analysis between these two groups were performed.

Abbreviations: LIHC, Liver Hepatocellular Carcinoma; LGG, Brain Lower Grade Glioma; MESO, Mesothelioma; BLCA, Bladder Urothelial Carcinoma; CESC, Cervical squamous cell carcinoma and endocervical adenocarcinoma; UVM, Uveal Melanoma; HNSC, Head and Neck squamous cell carcinoma; BRCA, Breast invasive carcinoma; KIRP, Kidney renal papillary cell carcinoma; ACC, Adrenocortical carcinoma; NA, Not Available; NS, No significance. KICH, Kidney Chromophobe; LUSC, Lung squamous cell carcinoma; PAAD, Pancreatic adenocarcinoma; PRAD, Prostate adenocarcinoma.

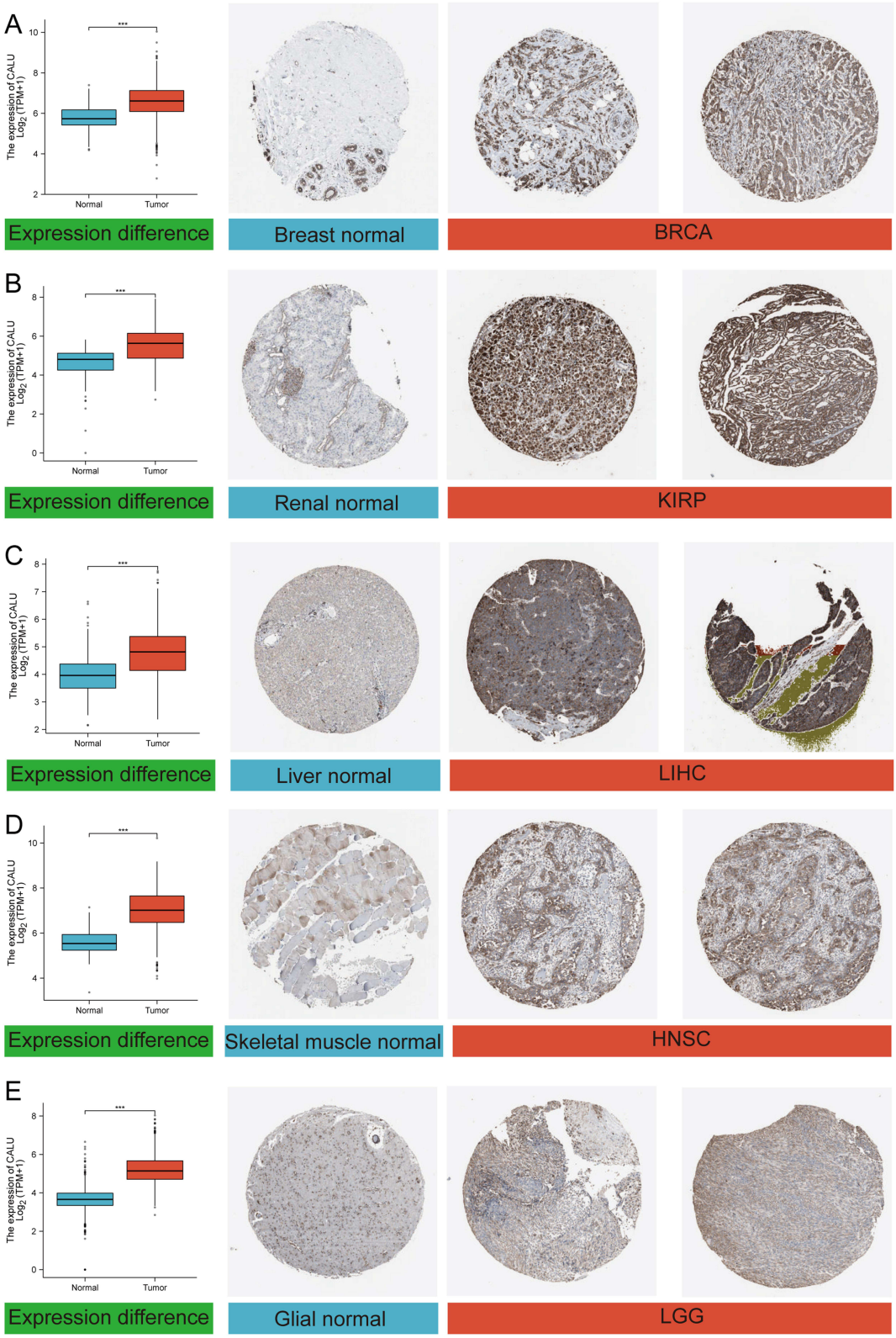

Figure 4 CALU Immunohistochemistry data (HPA) and mRNA expression data (TCGA) in different tumors. (**A**) BRCA, (**B**) KIRP, (**C**) LIHC, (**D**) HNSC, and (**E**) LGG. ***p< 0.001.

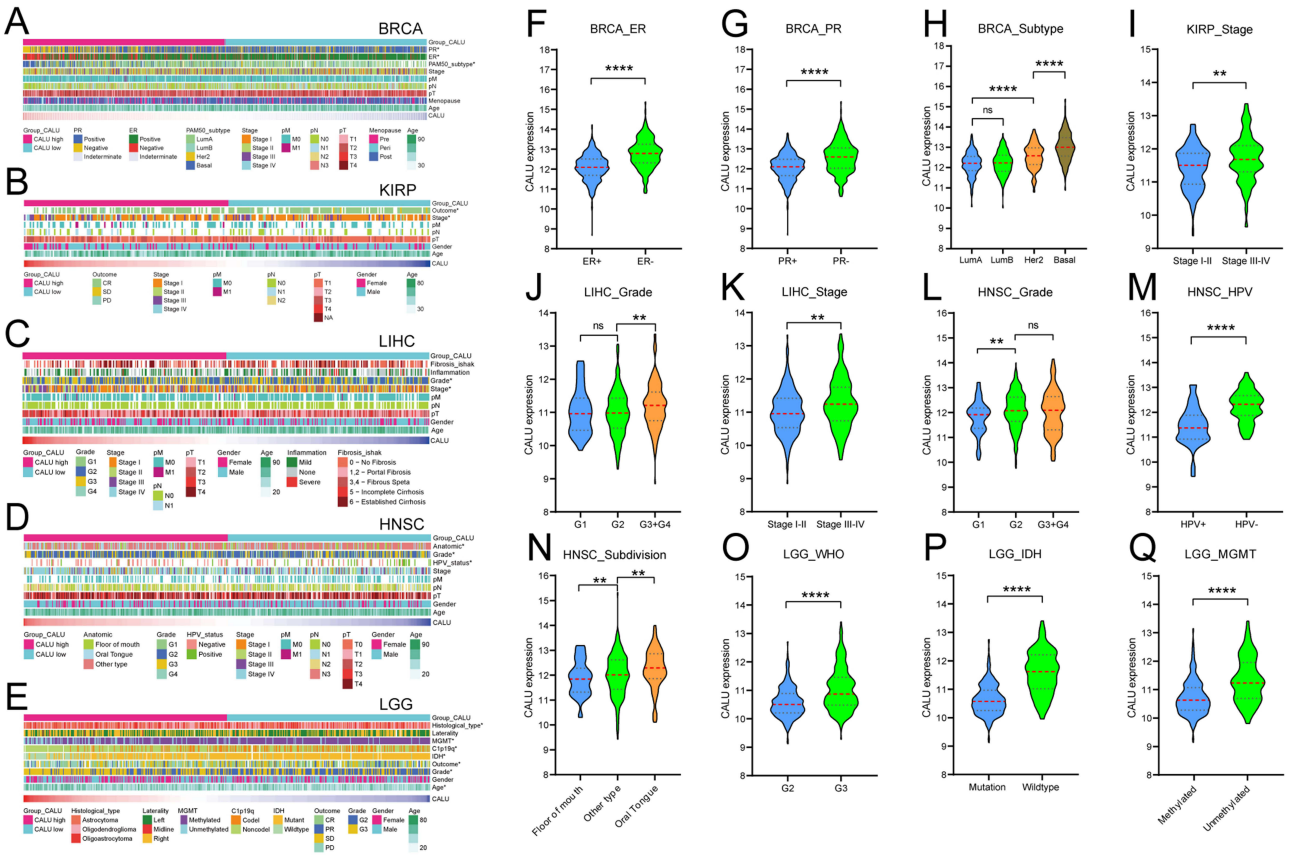

Figure 5 Clinical characteristics analysis of CALU in different tumors. (**A**) BRCA, (**B**) KIRP, (**C**) LIHC, (**D**)HNSC, (**E**)LGG. (**F–Q**) Analysis of CALU mRNA expression among distinct clinical characteristics in diverse tumor types. **p< 0.01; ****p< 0.0001.

primary mechanism driving *CALU* alterations, particularly in BRCA (Supplementary Figure 1A). *CALU* mutations were relatively rare, with two key mutations identified: R111L and P182A (Supplementary Figure 1B).

To further explore the regulation of *CALU* expression, the correlation between DNA methylation and *CALU* expression was analyzed across 33 TCGA tumors. Most patients exhibited low levels of *CALU* DNA methylation (Supplementary Figure 1C). Whole-genome sequencing, methylation, and transcriptome data were also collected from patients with BRCA, KIRP, LIHC, HNSC, and LGG (Supplementary Table 2). The analysis revealed a positive correlation between *CALU* mRNA levels and copy number variations in these five tumors (Supplementary Figure 1D–H, red points, $p < 0.05$), while no significant correlation was found between *CALU* expression and promoter methylation levels (Supplementary Figure 1D–H, blue points, $p > 0.05$).

CALU Expression Levels are Significantly Correlated with CAFs

The TIMER database was employed to explore the correlation between *CALU* expression levels and various TME cells. Among all cell types, CAFs exhibited the strongest association with *CALU* (Figure 6A). Three different algorithms—MCPCOUNTER, EPIC, and TIDE—consistently demonstrated a high correlation between *CALU* and CAFs across most cancer types. *CALU* showed a positive correlation with CAFs, endothelial cells, and neutrophil infiltration, while a negative correlation was observed with T cell follicular helper (Tfh) infiltration. Multiple algorithms, including MCPCOUNTER, EPIC, TIMER, XCELL, CIBERSORT, and CIBERSORT-AS, indicated a positive correlation between *CALU* and macrophage infiltration, whereas TIDE and XCELL algorithms revealed a negative correlation with M2 macrophage infiltration. Regarding Common Lymphoid Progenitor cells (CLP), Myeloid-Derived Suppressor Cells (MDSCs), and NK T cells, only one of the algorithms demonstrated a relationship between *CALU* and the respective

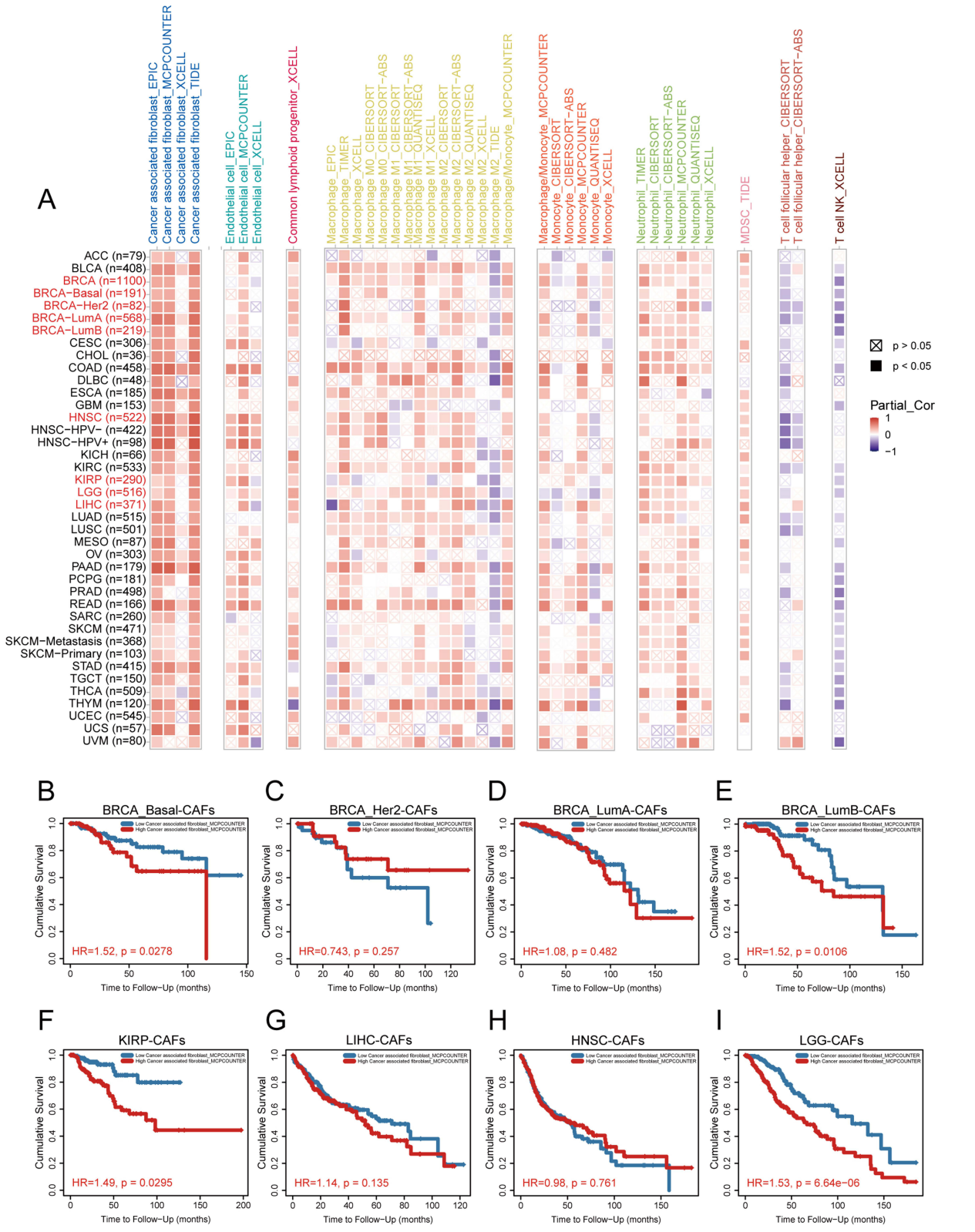

Figure 6 Correlation between CALU expression and tumor microenvironment cells utilizing bulk RNA-seq. (**A**) The correlation between CALU mRNA expression and various stromal cells and immune cells was analyzed by timer database. The impact of cancer-associated fibroblast (CAFs) cells with varying degrees of infiltration on the prognosis of BRCA-Basal (**B**), BRCA-Her2(**C**), BRCA-LumA(**D**), BRCA-LumB(**E**), KIRP(**F**), LIHC(**G**), HNSC(**H**), and LGG(**I**) is being examined.

cell infiltration. Specifically, *CALU* was positively correlated with CLP and MDSC infiltration but negatively correlated with NK T cell infiltration.

The impact of varying levels of CAF infiltration on the prognosis of BRCA and other tumors was further investigated (Figure 6B–I). The results indicated that patients with low CAF infiltration had significantly better prognoses in Basal subtype breast cancer (HR = 1.52, p = 0.0278), LumB subtype breast cancer (HR = 1.52, p = 0.0106), KIRP (HR = 1.49, p = 0.0295), and LGG (HR = 1.53, p = 6.64e-6). To further validate the relationship between *CALU* and CAFs, single-cell sequencing data were analyzed. Single-cell datasets were selected from samples of patients with BRCA, Glioma, HNSC, and LIHC or animal models, resulting in 15 datasets (Figure 7A). *CALU* expression was examined across various cell types, revealing significantly elevated *CALU* levels in fibroblasts, excluding malignant cells, within tumor tissues (Figure 7A). *CALU* expression was quantified in different cell types, including immune cells, stromal cells, and malignant cells, with violin plots illustrating expression levels across five datasets, including BRCA. The data consistently showed that *CALU* was predominantly expressed in stromal cells, such as CAFs and endothelial cells, in BRCA, HNSC, and LIHC (Figure 7B–F). Notably, higher *CALU* expression was also detected in malignant cells, which aligns with the findings from bulk RNA-seq analysis.

CALU is Related to EMT of CAFs and Malignant Cells

To investigate the biological role of *CALU* expression across various tumor types, GSEA and GSVA analyses were performed. Several established tumor pathways were selected, and the association between *CALU* and these pathways was analyzed using the GSEA database. The results demonstrated that elevated *CALU* expression was most strongly correlated with the EMT pathway across multiple tumor types. In particular, BRCA, LIHC, HNSC, and LGG exhibited a significant positive correlation between *CALU* expression and the EMT pathway (Figure 8A, $p < 0.05$).

In BRCA, *CALU* expression levels showed a robust correlation with EMT scores (Figure 8B, $R = 0.40$, $p < 0.05$), with similarly significant correlations observed in LGG, LIHC, HNSC, and KIRP (Figure 8B, $p < 0.05$). To explore this relationship further, the expression correlation between *CALU* and a 15-gene EMT marker set[28] was analyzed using transcriptomic data from the TCGA-BRCA project (Figure 8C and D). The analysis revealed a strong positive association

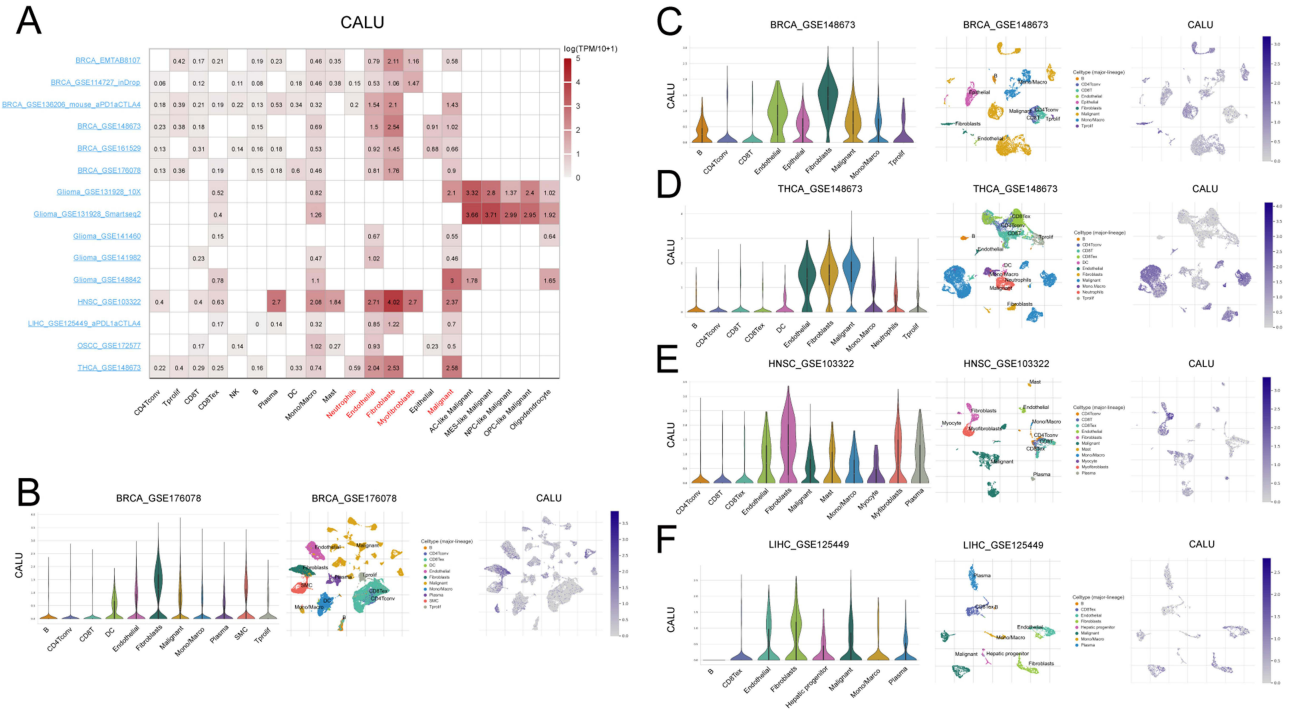

Figure 7 CALU is highly expressed in tumor stromal cells compared to other cells. (**A**) Heatmap of CALU expression levels by cell type in 15 single cell datasets including BRCA. (**B**) BRCA_GSE176078; (**C**) BRCA_GSE148673; (**D**) THCA_GSE148673; (**E**) HNSC_GSE103322; (**F**) LIHC_GSE125449.

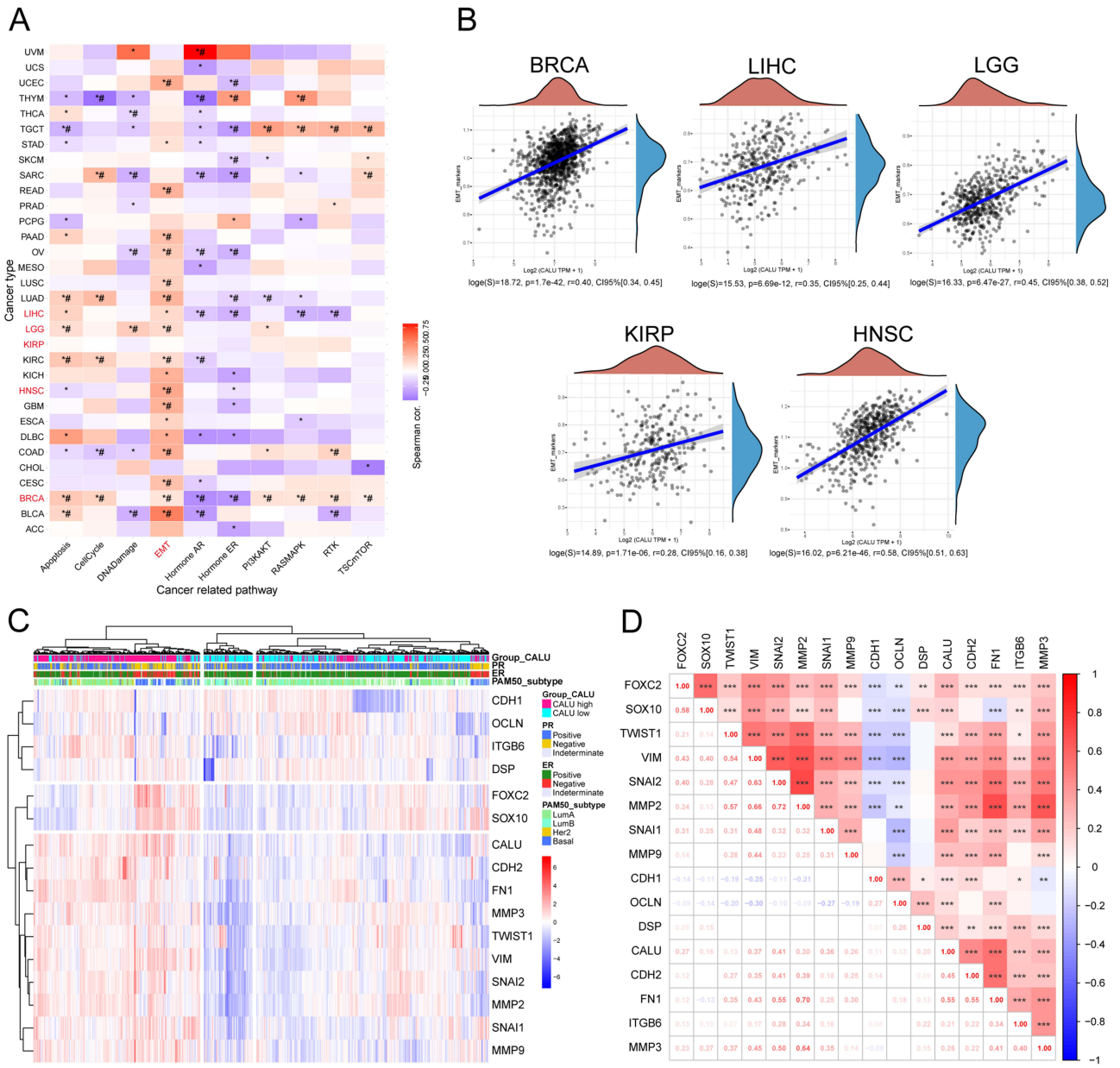

Figure 8 CALU is closely related to the EMT process in BRCA. (**A**) Correlation analysis between CALU expression level and different signaling pathways in various cancers. (**B**) Correlation analysis between CALU and EMT scores in BRCA and other 4 tumors. (**C** and **D**) Heatmap and correlation analysis of CALU expression and EMT marker genes' expression.*: p<0.05; #: FDR<0.05.

between *CALU* and key mesenchymal markers, including *FN1, CDH2, SNAI1, SNAI2*, and *VIM*. Additionally, a substantial correlation between *EMT markers* and *CALU* expression was observed across the other four tumor types (Figure 8D, r = 0.55, p < 0.001; Supplementary Figure 2).

To validate these findings, three BRCA single-cell datasets—BRCA_GSE176078, BRCA_GSE148673, and BRCA_GSE114727_inDrop—were analyzed (Figure 9A–C). These datasets indicated markedly higher EMT progression in fibroblasts and myofibroblasts, with considerable EMT activity also detected in malignant cells and mononuclear macrophages in the BRCA_GSE148673 dataset. Notably, consistent expression patterns of *FN1* and *CALU* were observed across different cell types in all three BRCA datasets, with both genes highly expressed in fibroblasts, endothelial cells, and mononuclear macrophages (Figure 9A–C, right). These results suggest that CAFs play a pivotal

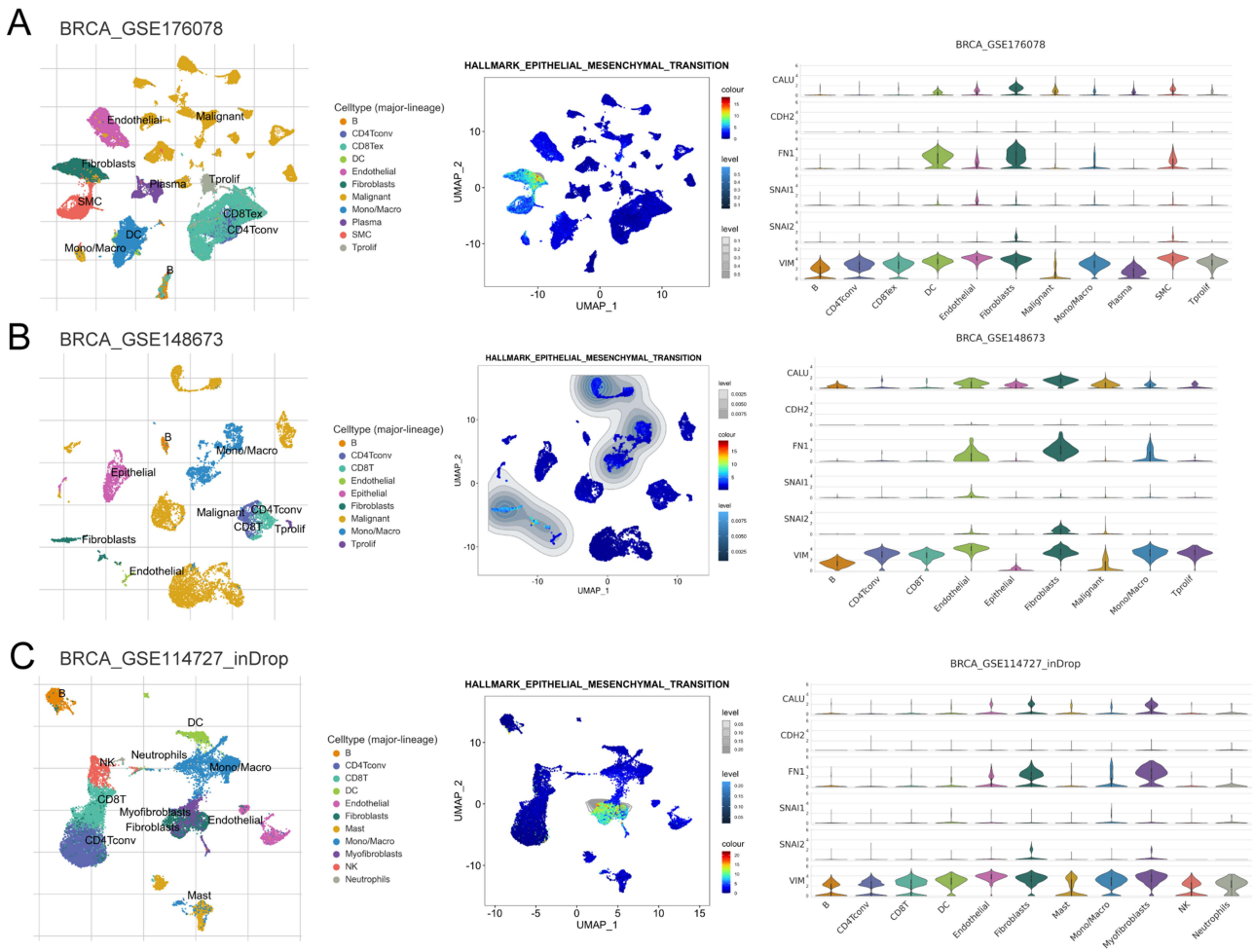

Figure 9 Visualization of EMT signatures in the t-SNE map of 3 scRNA-seq databases from BRCA. t-SNE plots of different cell types, EMT feature UMAP plots, and violin plots showing the expression of CALU and EMT markers, derived from the GSE176078 (**A**), GSE148673 (**B**), and GSE114727 (**C**) datasets, respectively.

role in driving the EMT process across multiple tumors, including BRCA, and that *CALU* is significantly and positively correlated with EMT progression.

CALU is Highly Expressed in BRCA, and Knockdown of CALU Can Reverse EMT and Inhibit Cell Migration

An analysis of *CALU* differential expression in BRCA cell lines revealed significant upregulation in triple-negative breast cancer cell lines MDA-231 and MDA-468 compared to the normal breast cell line MCF-10A (Figure 10A–C). This finding aligns with previous results (Figures 1 and 3A). To further investigate the role of *CALU* in BRCA, *CALU* knockdown was performed in MDA-231 and MDA-468 cell lines (Figure 10D–F). Three siRNAs targeting *CALU* were designed, with siR-*CALU*#1 selected for subsequent experiments (Figure 10D). Following transfection with siR-*CALU* #1, both MDA-231 and MDA-468 exhibited significantly reduced migration (Figure 10G–I, $p < 0.01$). Additionally, siR-*CALU*#1-transfected MDA-231 and MDA-468 cells showed decreased expression of *Vimentin*, N-*Cadherin*, and *Snail*, alongside a marked upregulation of *E-Cadherin* expression (Figure 10J–L). Figure 10E, F, K and L are the results of quantitative analysis of WB gel map respectively.

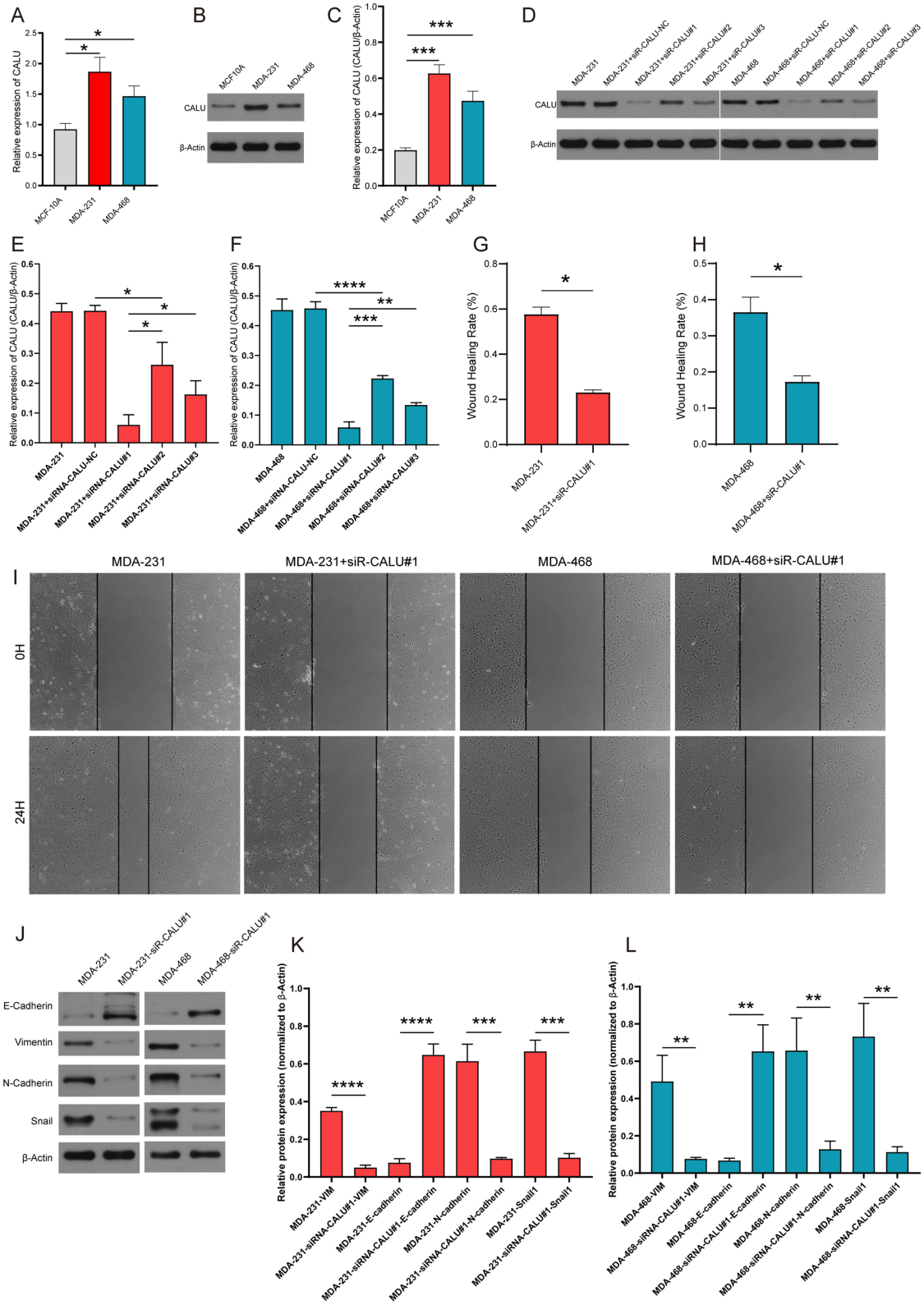

Figure 10 Knockdown of CALU inhibits the EMT process in breast cancer cells. The expression of CALU in triple-negative breast cancer cell lines MDA-231 and MDA-468 was significantly higher than that in normal breast cell line MCF10A, both in mRNA(**A**) and protein (**B** and **C**). (**D**–**F**) Detection of protein expression of CALU after transfection with different small interfering RNAs targeting CALU. (**G**–**I**) Wound healing assay of MDA-231 and MDA-468 cell lines after transfection of siR-CALU#1. (**J**–**L**) Detection of EMT marker gene expression in MDA-231 and MDA-468 cell lines before and after knockdown. *p< 0.05; **p< 0.01; ***p< 0.001; ****p< 0.0001.

CALU protein expression is significantly higher in breast cancer tissues and accompanied by changes in EMT marker gene expression

CALU protein expression was notably higher in breast cancer tissues and was accompanied by alterations in EMT marker gene expression. IHC and IF staining were performed on eight pairs of BRCA samples, each containing tumor and adjacent non-tumorous tissue, to validate *CALU* expression. Results demonstrated a significant increase in *CALU* expression in tumor tissues (Figure 11A and B). Additionally, IHC analysis of EMT markers, revealed elevated expression of N-Cadherin, Vimentin, and Snail in tumor tissues, while E-Cadherin expression remains unchanged (Figure 11B and C). This may be related to the low expression of E-cadherin in triple-negative breast cancer. Immunofluorescence staining further confirmed upregulated *CALU* expression in some CD3-positive cells and tumor cells, as well as in a subset of fibroblasts (Figure 11D and E). In tumor tissues, an interlaced arrangement of tumor cells and CAFs was also observed.

Discussion

Recent advancements in CAF-based therapies aimed at enhancing anti-tumor immunity have shown promising clinical potential, particularly in solid tumors such as melanoma, breast cancer, pancreatic cancer, and colorectal cancer.[29–32] These therapeutic strategies include anti-CAF CAR-T cell therapy, targeting key CAF pathways, and reprogramming CAFs.[33] However, their application remains constrained by the heterogeneity of CAFs and the absence of reliable markers. The availability of multi-omics tumor sequencing data has significantly enhanced our ability to perform comprehensive studies on gene functions in tumors.[34,35] Our research leverages such multi-omics data to explore the role of CALU across different tumor types, thereby advancing our understanding of its function within the TME.

Consistent with previous findings,[22] our study confirms the elevated expression of CALU in various tumors, including BRCA, HNSC, KIRP, LGG, and LIHC, and its association with poor prognosis. Notably, Yang et al[22] identified CALU as a prognostic biomarker in LGG, a finding our research supports while extending its relevance to additional tumor types. While Yang et al primarily focused on LGG, our investigation highlights CALU's broader significance, suggesting its potential as a universal prognostic marker across multiple cancers. This is particularly evident in breast cancer, where high CALU expression was observed in ER- and PR-negative patients, indicating a possible correlation between CALU expression and hormone receptor status. Moreover, CALU expression was highest in the basal-like subtype of breast cancer, with in vitro studies confirming increased CALU expression in triple-negative breast cancer cells, suggesting its utility as a marker for distinguishing basal-like breast cancer from other subtypes.

Initially, we conducted an analysis of CALU expression levels in various tumor cell lines utilizing the CCLE database (Supplementary Figure 3). Interestingly, we observed the highest expression levels in the LGG cell line, while comparatively lower levels were detected in the HNSC cell line. In HNSC, an intriguing observation was the inverse relationship between HPV positivity and CALU expression, with lower CALU levels in HPV-positive patients, a finding that merits further investigation. Additionally, elevated CALU expression in tongue tumor subtypes may serve as a predictive marker for this specific subtype. In KIRP, high CALU expression correlated with poor prognosis, reinforcing its potential as a prognostic indicator in this cancer type. In our breast cancer analysis, CALU demonstrated significant associations with various clinical features, particularly with the growing global incidence of breast cancer, highlighting the need for a deeper focus on CALU's role in this disease. Our study also introduces a novel perspective by exploring the interaction mechanisms between CALU in tumor cells and CAFs, offering new insights into its role in the TME.

CALU is strongly associated with CAF infiltration, with the TME, particularly CAFs, playing a critical role in tumor invasion and metastasis.[34,36–39] Tumor cells enhance their motility through interactions with CAFs, which, in turn, suppress antitumor immune functions by releasing collagen. Kunita et al[16] demonstrated that in lung cancer, CAFs secrete CALU via a TGF-β-induced miR-21 expression axis, promoting tumor proliferation and metastasis. This suggests that CALU is actively involved in signaling between malignant cells and stromal cells, underscoring its complex role in tumor progression. TIMER immune infiltration score analysis reveals a significant positive correlation between CALU expression and CAF scores across nearly all cancer types. Additionally, CALU expression correlates positively with the

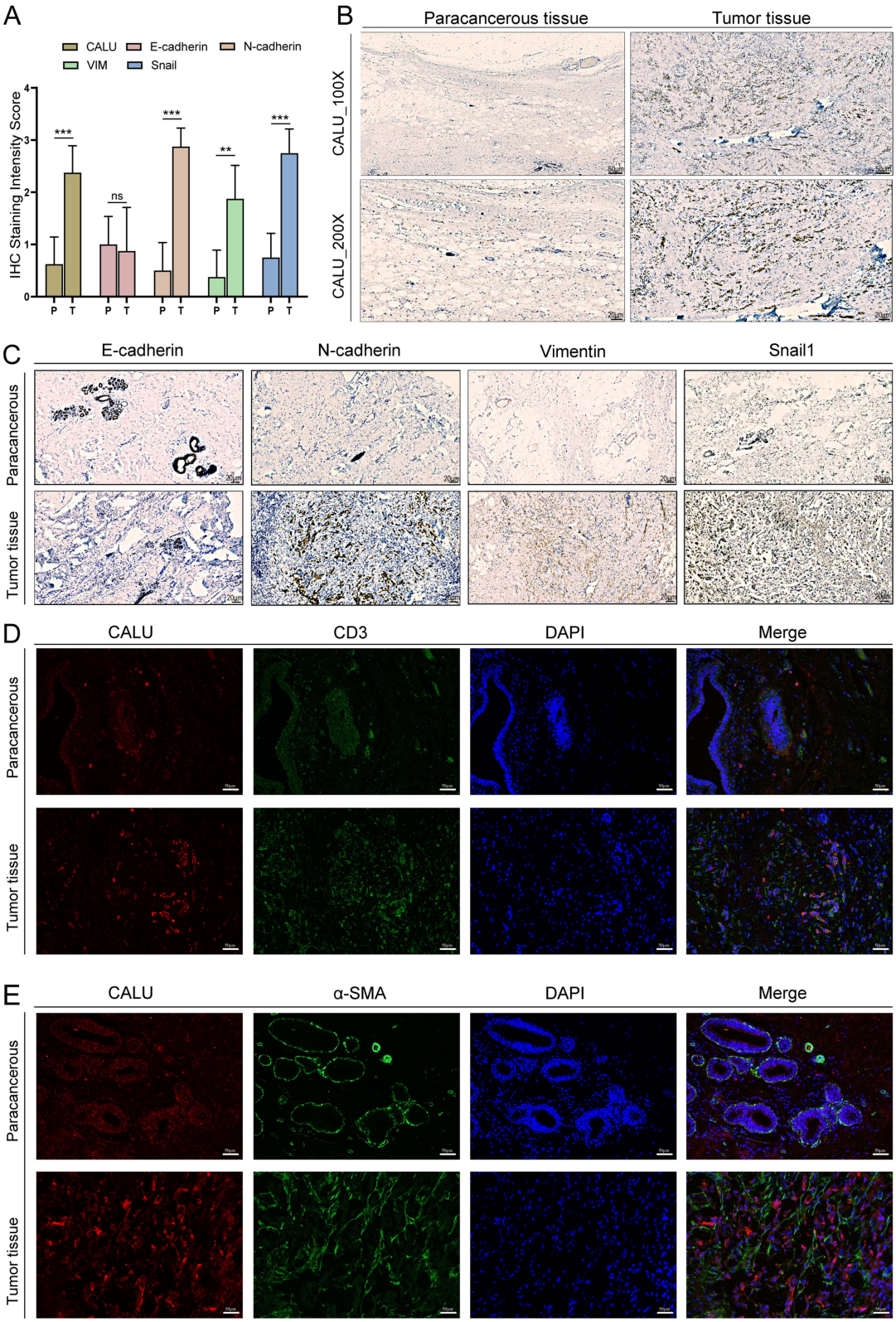

Figure 11 Validation of CALU, EMT marker genes, CD3 and α-SMA in breast cancer samples. (**A**) IHC staining scores for CALU and EMT markers from 8 TNBC patients. (**B** and **C**) IHC staining results of CALU, E-cadherin, N-cadherin, Vimentin and Snail1 in TNBC tissues. (**D**) IF staining results of CALU and CD3 in breast cancer tissue. (**E**) IF staining results of CALU and α-SMA in breast cancer tissue.**p< 0.01; ***p< 0.001.

infiltration of endothelial cells, neutrophils, CLPs, and MDSCs, while showing a negative correlation with T cell and natural killer (NK) cell infiltration.

Our findings also indicate that patients with basal-like BRCA, LumB-type BRCA, KIRP, and CAF-infiltrated LGG exhibit significantly worse prognoses, consistent with previous studies[41–43]. Single-cell analysis reveals elevated CALU expression in both fibroblasts and malignant cells in tumors such as BRCA, aligning with results from bulk RNA-seq analysis. Furthermore, our study highlights the active communication between malignant cells and stromal cells, including CAFs, within the TME (Supplementary Figure 4). Immunofluorescence staining of clinical samples showed high CALU expression in breast cancer tumor cells and CAFs, with some CD3-positive cells also expressing CALU, reflecting the complexity of cellular interactions in the TME. These results suggest that CALU is highly expressed in both CAFs and malignant cells, although the precise mechanisms by which it promotes tumor progression remain unclear. By emphasizing CALU's importance within the stroma-related microenvironment, our study extends previous research that primarily focused on its role in tumor cells.

Our findings regarding CALU's involvement in EMT are consistent with earlier studies,[40–43] which identify EMT as a central mechanism in cancer metastasis. However, our research further clarifies this process by showing that the interaction between CALU and CAFs is instrumental in promoting EMT and tumor progression. GSEA pathway analysis demonstrates a strong correlation between CALU and EMT across various cancers, with a positive relationship between CALU expression and EMT scores. In bulk analysis of breast cancer transcriptomes, CALU expression was positively correlated with key stromal markers, including FN1, CDH2, SNAI1, SNAI2, and VIM. Subsequent analysis of BRCA single-cell datasets further confirmed these results. Collectively, these results suggest that CALU actively participates in promoting EMT in multiple tumors, although further research is required to fully elucidate the specific mechanisms through which CALU influences tumor progression.

Our in vitro experiments strongly support the hypothesis that CALU plays a pivotal role in the EMT process. Specifically, CALU knockdown in TNBC cell lines resulted in a reversal of EMT, accompanied by a reduction in migratory capacity. These results suggest that CALU may facilitate tumor progression by enhancing tumor cell migration through the EMT mechanism. Immunohistochemical staining of paraffin-embedded sections further corroborated these findings, demonstrating elevated expression of CALU and EMT marker genes in TNBC tumor cells.

Of note, Mazzorana et al[44] identified that CALU performs its calcium-regulating functions by binding to SERCA and ryanodine receptors within the cytoplasm. In various cancers, including TNBC, calcium (Ca^{2+}) plays a vital role in tumor proliferation, migration, and invasion.[45–47] Chen et al[13] demonstrated that Cab45, another CREC family member, promotes tumor cell proliferation in glioblastoma multiforme (GBM) through the calcium-NFAT pathway, suggesting that CALU may similarly drive tumor cell proliferation via calcium-regulated pathways.

However, several limitations of our study should be acknowledged. Due to experimental constraints, the research primarily focused on TNBC and did not extensively examine the role of CALU in other breast cancer subtypes, such as HER2-positive or luminal types. Additionally, the immunohistochemical analysis was conducted on samples from only eight patients with TNBC. While these results provide valuable preliminary insights, the small sample size limits the generalizability of our conclusions. Furthermore, although our study indicates a close association between CALU and the TME, particularly with CAFs, this conclusion is drawn primarily from immunofluorescence results, which limit the rigor of the finding. These limitations underscore the need for future research to expand on our observations and deepen the understanding of CALU's role in cancer biology.

Previous research indicates that CALU may exert a pan-cancer effect, marked by its elevated expression across multiple tumor types and its correlation with poorer prognosis. Although this study concentrates on triple-negative breast cancer, future investigations could expand to other breast cancer subtypes or malignancies to further establish CALU's potential as both a prognostic marker and a therapeutic target. CALU exhibits diverse functions, not only being linked to EMT but also playing a crucial role in calcium ion homeostasis and the regulation of cell proliferation. To deepen the understanding of CALU's involvement in tumor progression, especially in the context of interactions between tumor cells and CAFs, future studies should incorporate additional functional assays and mechanistic analyses.

Conclusion

This study conducted an in-depth analysis of the correlation between CALU expression and clinical characteristics across various tumor types, establishing CALU as an independent prognostic marker in multiple malignancies. By rigorously analyzing transcriptome and single-cell sequencing datasets, supported by experimental validation, the upregulation of CALU in BRCA was confirmed, demonstrating its role in promoting tumor cell migration through the facilitation of the EMT process. These findings provide new insights into CALU's involvement in tumor progression and open avenues for the development of more targeted and personalized therapeutic strategies.

Data Sharing Statement

This study involved an analysis of publicly accessible datasets, which can be accessed via the following links: GTEx (https://www.gtexportal.org/), cBioPortal (http://www.cbioportal.org), TCGA (https://portal.gdc.cancer.gov/), GSVA (https://www.cancerrxgene.org/), TISCH database (http://tisch.comp-genomics.org/), and TIMER (http://timer.cistrome.org/).

Ethics Approval and Consent to Participate

No animal studies are presented in this manuscript.

The studies involving humans were approved by The First Affiliated Hospital of Zhejiang Chinese Medical University (No: 2022-KL-179-01) (October 28, 2022). The studies were conducted in accordance with the local legislation and institutional requirements. The human samples used in this study were acquired from primarily isolated as part of your previous study for which ethical approval was obtained. Written informed consent for participation was not required from the participants or the participants' legal guardians/next of kin in accordance with the national legislation and institutional requirements.

No potentially identifiable images or data are presented in this study.

Author Contributions

All authors made a significant contribution to the work reported, whether that is in the conception, study design, execution, acquisition of data, analysis and interpretation, or in all these areas; took part in drafting, revising or critically reviewing the article; gave final approval of the version to be published; have agreed on the journal to which the article has been submitted; and agree to be accountable for all aspects of the work.

Funding

The study design, data collection, data analysis, manuscript preparation, and publication decisions of this work were supported by Zhejiang Province Traditional Chinese Medicine Science and Technology Project (No. 2024ZR015 by YB. H., No. 2023ZL056 by ZZ.Z), Zhejiang Province Medical and Health Science and Technology Project (No. 2024KY1201 by YB.H, 2024KY1225 by C.W, 2024KY1213 by ZZ.Z), the Research Project of Zhejiang Chinese Medical University (No. 2022JKZKTS26 by YB.H, No. 2022JKJNTZ16 by SL.C, No. 2022JKJNTZ23 by C.W, No. 2023JKJNTZ10 by CF. Z). We extend our gratitude to Bullet Edits for their assistance in refining the language of this manuscript.

Disclosure

The authors declare no financial non-financial or competing interests.

References

1. Siegel RL, Miller KD, Wagle NS, Jemal A. Cancer statistics, 2023. *CA*. 2023;73(1):17–48. doi:10.3322/caac.21763
2. Siegel RL, Miller KD, Jemal A. Cancer statistics, 2019. *CA*. 2019;69(1):7–34. doi:10.3322/caac.21551
3. Li YQ, Sun FZ, Li CX, et al. RARRES2 regulates lipid metabolic reprogramming to mediate the development of brain metastasis in triple negative breast cancer. *Military Med Res*. 2023;10(1):34. doi:10.1186/s40779-023-00470-y
4. Wang Y, Li Y, Jing Y, et al. Tubulin alpha-1b chain was identified as a prognosis and immune biomarker in pan-cancer combing with experimental validation in breast cancer. *Sci Rep*. 2024;14(1):8201. doi:10.1038/s41598-024-58982-z

5. Mao Y, Keller E, Garfield D, Shen K, Wang J. Stromal cells in tumor microenvironment and breast cancer. *Cancer Metastasis Rev*. 2013;32:303–315. doi:10.1007/s10555-012-9415-3
6. Cohen N, Shani O, Raz Y, et al. Fibroblasts drive an immunosuppressive and growth-promoting microenvironment in breast cancer via secretion of Chitinase 3-like 1. *Oncogene*. 2017;36:4457–4468. doi:10.1038/onc.2017.65
7. Xu H, Xu B. Breast cancer: epidemiology, risk factors and screening. *CJCR*. 2023;35(6):565–583. doi:10.21147/j.issn.1000-9604.2023.06.02
8. Hu D, Li Z, Zheng B, et al. Cancer-associated fibroblasts in breast cancer: challenges and opportunities. *Cancer Commun*. 2022;42:401–434. doi:10.1002/cac2.12291
9. Xing S, Hu K, Wang Y. Tumor immune microenvironment and immunotherapy in non-small cell lung cancer: update and new challenges. *Aging Dis*. 2022;13(6):1615–1632. doi:10.14336/AD.2022.0407
10. Tsuji A, Kikuchi Y, Sato Y, et al. A proteomic approach reveals transient association of reticulocalbin-3, a novel member of the CREC family, with the precursor of subtilisin-like proprotein convertase, PACE4. *Biochem J*. 2006;396(1):51–59. doi:10.1042/BJ20051524
11. Sahoo SK, Kim T, Kang GB, Lee JG, Eom SH, Kim DH. Characterization of calumenin-SERCA2 interaction in mouse cardiac sarcoplasmic reticulum *. *J Biol Chem*. 2009;284(45):31109–31121. doi:10.1074/jbc.M109.031989
12. von Blume J, Alleaume AM, Kienzle C, Carreras-Sureda A, Valverde M, Malhotra V. Cab45 is required for Ca2+-dependent secretory cargo sorting at the trans-Golgi network. *J Cell Biol*. 2012;199(7):1057–1066. doi:10.1083/jcb.201207180
13. Chen L, Xu S, Xu Y, et al. Cab45S promotes cell proliferation through SERCA2b inhibition and Ca2+ signaling. *Oncogene*. 2016;35(1):35–46. doi:10.1038/onc.2015.56
14. Chen L, Xu S, Liu L, et al. Cab45S inhibits the ER stress-induced IRE1-JNK pathway and apoptosis via GRP78/BiP. *Cell Death Dis*. 2014;5(5):e1219. doi:10.1038/cddis.2014.193
15. Nagano K, Imai S, Zhao X, et al. Identification and evaluation of metastasis-related proteins, oxysterol binding protein-like 5 and calumenin, in lung tumors. *Int j Oncol*. 2015;47(1):195–205. doi:10.3892/ijo.2015.3000
16. Kunita A, Morita S, Irisa TU, et al. MicroRNA-21 in cancer-associated fibroblasts supports lung adenocarcinoma progression. *Sci Rep*. 2018;8(1):8838. doi:10.1038/s41598-018-27128-3
17. Nasri Nasrabadi P, Nayeri Z, Gharib E, et al. Establishment of a CALU, AURKA, and MCM2 gene panel for discrimination of metastasis from primary colon and lung cancers. *PLoS ONE*. 2020;15(5):e0233717. doi:10.1371/journal.pone.0233717
18. Vorum H, Hager H, Christensen BM, Nielsen S, Honoré B. Human calumenin localizes to the secretory pathway and is secreted to the medium. *Exp Cell Res*. 1999;248(2):473–481. doi:10.1006/excr.1999.4431
19. Hansen GAW, Vorum H, Jacobsen C, Honoré B. Calumenin but not reticulocalbin forms a Ca2+-dependent complex with thrombospondin-1. A potential role in haemostasis and thrombosis. *Mol Cell Biochem*. 2009;320(1):25–33. doi:10.1007/s11010-008-9895-1
20. Østergaard M, Hansen GAW, Vorum H, Honoré B. Proteomic profiling of fibroblasts reveals a modulating effect of extracellular calumenin on the organization of the actin cytoskeleton. *Proteomics*. 2006;6(12):3509–3519. doi:10.1002/pmic.200500686
21. Du Y, Miao W, Jiang X, et al. The epithelial to mesenchymal transition related gene calumenin is an adverse prognostic factor of bladder cancer correlated with tumor microenvironment remodeling, gene mutation, and ferroptosis. *Front Oncol*. 2021;11:683951. doi:10.3389/fonc.2021.683951
22. Yang Y, Wang J, Xu S, Shi F, Shan A. Calumenin contributes to epithelial-mesenchymal transition and predicts poor survival in glioma. *Transl Neurosci*. 2021;12(1):67–75. doi:10.1515/tnsci-2021-0004
23. Ji X, Tian X, Feng S, et al. Intermittent F-actin perturbations by magnetic fields inhibit breast cancer metastasis. *Research*. 2023;6:0080. doi:10.34133/research.0080
24. Wang Y, Bi X, Luo Z, Wang H, Ismtula D, Guo C. Gelsolin: a comprehensive pan-cancer analysis of potential prognosis, diagnostic, and immune biomarkers. *Front Genet*. 2023;14. doi:10.3389/fgene.2023.1093163.
25. Wang L, Saci A, Szabo PM, et al. EMT- and stroma-related gene expression and resistance to PD-1 blockade in urothelial cancer. *Nat Commun*. 2018;9(1):3503. doi:10.1038/s41467-018-05992-x
26. Szebényi K, Füredi A, Bajtai E, et al. Effective targeting of breast cancer by the inhibition of P-glycoprotein mediated removal of toxic lipid peroxidation byproducts from drug tolerant persister cells. *Drug Resist Updates*. 2023;71:101007. doi:10.1016/j.drup.2023.101007
27. Shen W, Song Z, Zhong X, et al. Sangerbox: a comprehensive, interaction-friendly clinical bioinformatics analysis platform. *iMeta*. 2022;1(3):e36. doi:10.1002/imt2.36
28. Gibbons DL, Creighton CJ. Pan-cancer survey of epithelial–mesenchymal transition markers across the cancer genome atlas. *Dev Dyn*. 2018;247(3):555–564. doi:10.1002/dvdy.24485
29. Barrett R, Puré E. Cancer-associated fibroblasts: Key determinants of tumor immunity and immunotherapy. *Current Opinion Immunol*. 2020;64:80–87. doi:10.1016/j.coi.2020.03.004
30. Liu T, Han C, Wang S, et al. Cancer-associated fibroblasts: an emerging target of anti-cancer immunotherapy. *J Hematol Oncol*. 2019;12(1):86. doi:10.1186/s13045-019-0770-1
31. Hegde M, Daimary UD, Kumar A, et al. STAT3/HIF1A and EMT specific transcription factors regulated genes: novel predictors of breast cancer metastasisSTAT3/HIF1A 和 EMT. *Gene*. 2022;818:146245. doi:10.1016/j.gene.2022.146245
32. Jafarinejad-Farsangi S, Moazzam-Jazi M, Naderi Ghale-noie Z, et al. Investigation of genes and pathways involved in breast cancer subtypes through gene expression meta-analysis. *Gene*. 2022;821:146328. doi:10.1016/j.gene.2022.146328
33. Glabman RA, Choyke PL, Sato N. Cancer-associated fibroblasts: tumorigenicity and targeting for cancer therapy. *Cancers*. 2022;14(16):3906. doi:10.3390/cancers14163906
34. Luo H, Xia X, Huang LB, et al. Pan-cancer single-cell analysis reveals the heterogeneity and plasticity of cancer-associated fibroblasts in the tumor microenvironment. *Nat Commun*. 2022;13(1):6619. doi:10.1038/s41467-022-34395-2
35. Schaduangrat N, Homdee N, Shoombuatong W. StackER: A novel SMILES-based stacked approach for the accelerated and efficient discovery of ERα and ERβ antagonists. *Sci Rep*. 2023;13(1):22994. doi:10.1038/s41598-023-50393-w
36. Szabo PM, Vajdi A, Kumar N, et al. Cancer-associated fibroblasts are the main contributors to epithelial-to-mesenchymal signatures in the tumor microenvironment. *Sci Rep*. 2023;13(1):3051. doi:10.1038/s41598-023-28480-9
37. Dong G, Chen P, Xu Y, Liu T, Yin R. Cancer-associated fibroblasts: key criminals of tumor pre-metastatic niche. *Cancer Lett*. 2023;566:216234. doi:10.1016/j.canlet.2023.216234

38. miao XX, yang LY, min CX, et al. Pan-cancer analysis identifies NT5E as a novel prognostic biomarker on cancer-associated fibroblasts associated with unique tumor microenvironment. *Front Pharmacol*. 2022;13:1064032. doi:10.3389/fphar.2022.1064032
39. Peng Z, Ye M, Ding H, Feng Z, Hu K. Spatial transcriptomics atlas reveals the crosstalk between cancer-associated fibroblasts and tumor microenvironment components in colorectal cancer. *J Transl Med*. 2022;20(1):1–13. doi:10.1186/s12967-022-03510-8
40. You J, Li M, Cao LM, et al. Snail1-dependent cancer-associated fibroblasts induce epithelial-mesenchymal transition in lung cancer cells via exosomes. *QJM*. 2019;112(8):581–590. doi:10.1093/qjmed/hcz093
41. Fedele V, Melisi D. Permissive state of EMT: the role of immune cell compartment. *Front Oncol*. 2020;10:587. doi:10.3389/fonc.2020.00587
42. Asif PJ, Longobardi C, Hahne M, Medema JP. The role of cancer-associated fibroblasts in cancer invasion and metastasis. *Cancers*. 2021;13 (18):4720. doi:10.3390/cancers13184720
43. Wiechec E, Magan M, Matic N, et al. Cancer-associated fibroblasts modulate transcriptional signatures involved in proliferation, differentiation and metastasis in head and neck squamous cell carcinoma. *Cancers*. 2021;13(13):3361. doi:10.3390/cancers13133361
44. Mazzorana M, Hussain R, Sorensen T. Ca-dependent folding of human calumenin. *PLoS One*. 2016;11(3):e0151547. doi:10.1371/journal.pone.0151547
45. Berzingi S, Newman MS, Yu HG. Altering bioelectricity on inhibition of human breast cancer cells. *Can Cell Inter*. 2016;16. doi:10.1186/s12935-016-0348-8.
46. Kim JH, sil HB, Heo W, et al. Calsequestrin 2 regulates proliferation, migration, and invasion in triple-negative breast cancer cells. *Cancer Res*. 2018;78(13_Supplement):33. doi:10.1158/1538-7445.AM2018-33
47. Lee D, Hong JH. Ca2+ signaling as the untact mode during signaling in metastatic breast cancer. *Cancers*. 2021;13(6):1473. doi:10.3390/cancers13061473